# 4 Earthquakes

*Much of what is known about earthquakes follows from study of the motion of the ground.*

Charles Richter, *Elementary Seismology*, 1958

## 4.1 Introduction

Seismology deals with the generation and propagation of seismic waves. Our initial focus has been on the propagation of seismic waves and how they can be used to study the interior of the earth. We now turn to the generation of seismic waves and how they are used to study earthquakes. This association is so strong that seismology is sometimes viewed as the science of earthquakes, rather than of elastic waves in the earth. Both definitions are used, but the latter has become more common because seismology is the primary tool used to investigate earth structure as well as earthquakes, whereas techniques other than elastic waves are also used to investigate earthquakes.

Earthquakes almost invariably occur on *faults*, surfaces in the earth on which one side moves with respect to the other. Typically, earthquakes occur on faults previously identified by geological mapping, which shows that motion across the fault has occurred in the past. Earthquakes that occur on land and close enough to the surface often leave visible ground breakage along the fault. For example, earthquakes occur along the San Andreas fault, which can be seen cutting across California for great distances (Fig. 4.1-1). One of these, the famous 1906 magnitude 7.8 San Francisco earthquake on the San Andreas fault was one of the first US earthquakes to be studied carefully. Contemporary accounts showed that several meters of relative motion occurred along several hundred kilometers of the San Andreas fault (Fig. 4.1-2).

The earthquake and the resultant fires did such damage (Fig. 1.2-10) that a study commission was formed. As part of the investigation, H. Reid proposed the *elastic rebound* theory of earthquakes on a fault. In this model, materials at distance on opposite sides of the fault move relative to each other, but friction on the fault "locks" it and prevents the sides from slipping (Fig. 4.1-3). Eventually the strain accumulated in the rock is more than the rocks on the fault can withstand, and the fault slips, resulting in an earthquake. The motion illustrated in this cartoon by an offset fence can sometimes be seen after earthquakes using other linear features, including rows of trees, railroad tracks, or roads (Fig. 4.1-4).

**Fig. 4.1-1** Aerial photograph of the San Andreas fault in the Carrizo Plain in California, seen from the south. Note the displacement of stream gullies as the Pacific plate (*near side*) has moved to the left (northwest) relative to North America. (Copyright John S. Shelton.)

The elastic rebound idea was a major conceptual breakthrough, because the faulting seen at the surface had been previously regarded as an incidental side effect of an earthquake, rather than its cause. Subsequently, earthquake studies have been widely pursued for several reasons. One is to understand the large-scale geological processes causing earthquakes. It

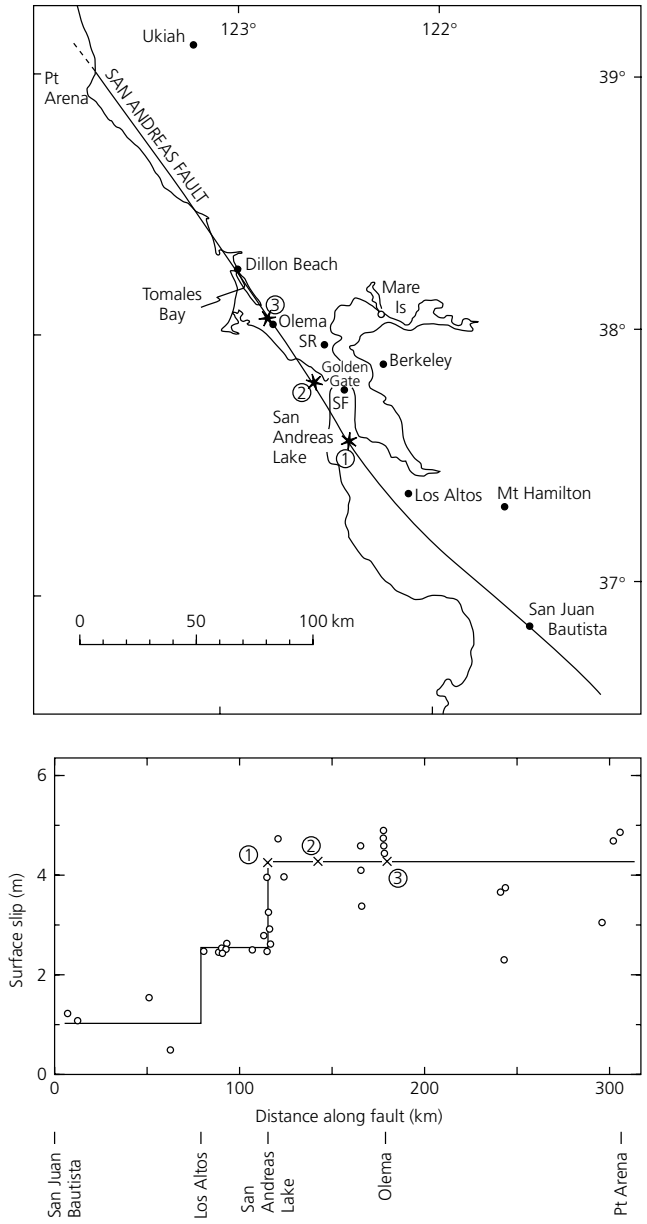


**Fig. 4.1-2** Map of the portion of the San Andreas fault that slipped in the 1906 San Francisco earthquake (*top*) and the amount of surface slip reported at various points along it (*bottom*). This slip is the distance by which the earthquake displaced originally adjacent features on opposite sides of the fault. (Boore, 1977. © Seismological Society of America. All rights reserved.)

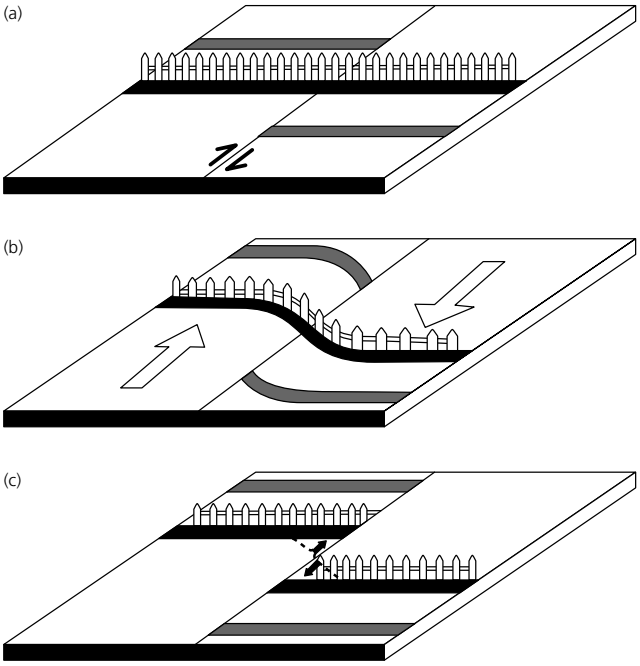


**Fig. 4.1-3** The elastic rebound model of earthquakes assumes that between earthquakes, material on the two sides of a fault undergoes relative motion. Because the fault is locked, features across it that were linear at time (a), such as a fence, are slowly deformed with time (b). Finally the strain becomes so great that the fault breaks in an earthquake, offsetting the features (time c). (Courtesy of S. Wesnousky.)

**Fig. 4.1-4** Displacement of crop rows resulting from slip along the Imperial fault, El Centro, California, on October 15, 1979. (Courtesy of the National Geophysical Data Center.)

turns out that earthquakes largely reflect the motions of lithospheric plates, and so provide valuable information about how and why plates move. For example, earthquakes on the San Andreas fault result from the steady motion between the North American and Pacific plates (Fig. 5.2-3). A second reason is to understand the fundamental physics of earthquake faulting. There are many unanswered questions about how and when faults break, even for earthquakes that occur near

the earth's surface, where data are relatively easy to gather. These issues are important for society because, as discussed in Chapter 1, knowledge of where and when earthquakes are likely, and of the expected ground motion during them, can help mitigate the risk they pose.

The largest earthquakes typically occur at plate boundaries. Using elastic rebound theory, we think of them as reflecting the most dramatic part of a process called the *seismic cycle*, which takes place on segments of the plate boundary over hundreds to thousands of years. During the *interseismic* stage, which makes up most of the cycle, steady motion occurs away from the fault but the fault itself is "locked," although some aseismic creep can also occur on it. Immediately prior to rupture there is the *preseismic* stage that can be associated with small earthquakes (foreshocks) or other possible precursory effects. The earthquake itself marks the *coseismic* phase during which rapid motion on the fault generates seismic waves. During these few seconds, meters of slip on the fault "catch up" with the few mm/yr of motion that occurred over hundreds of years away from the fault. Finally, a *postseismic* phase occurs after the earthquake, and aftershocks and transient afterslip occur for a period of years before the fault settles into its steady interseismic behavior again.

Studying this cycle is difficult because it extends for hundreds of years, so we do not have observations of it in any one place. Instead, we have observations from different places, which we assume can be combined to give a complete view of the process. It is far from clear how good that view is and how well our models represent its complexity. As a result, earthquake physics remains an active research area that integrates a variety of techniques. Most faults are identified from the earthquakes on them, and seismology is the primary tool used to study the motion during the earthquakes and infer the long-term nature of motion on the faults. Moreover, because earthquakes are such dramatic events, historical records of earthquakes are often available and provide data on the earthquake cycle for a given fault or fault segment. Field studies, both on land and under water, also provide information about the location, geometry, and history of faults. Geodetic measurements are used to study ground deformation before, during, and after earthquakes, and thus the processes associated with fault locking and afterslip. For oceanic regions and deep earthquakes, where geodetic and geological observations are not available, almost all of what we know about the earthquakes themselves comes from seismology. The results for individual earthquakes are then combined and integrated with those from other techniques, as discussed in the next chapter, to better understand how earthquakes in a given region reflect the large-scale tectonic processes that cause them.

Of these approaches, our primary focus in this book is the information that seismology provides about earthquakes. The arrival time of seismic waves at seismometers at different sites is first used to find the location of an earthquake, known as the *focus*, or *hypocenter*, using techniques discussed in Chapter 7. Next, as discussed in this chapter, the amplitudes and shapes of the radiated seismic waves are used to study the size of the earthquake, the geometry of the fault on which it occurred, and the direction and amount of slip. We introduce these techniques and discuss their applications, while leaving their derivation and details for more advanced treatments listed at the chapter's end.

It is worth bearing in mind that learning about earthquake faulting from the seismic waves that are generated is an inverse problem, like learning about earth structure from seismic waves. As discussed in Section 1.1.2, this means that studying seismic waves alone is limited in what it can tell about the earthquake process. We will see that the seismic waves radiated from an earthquake reflect the geometry of the fault and the motion on it, and so can give an excellent picture of the *kinematics* of faulting. However, they contain much less information about the actual physics, or *dynamics*, of faulting. In the next chapter, we discuss how seismological results are being combined with experimental and theoretical studies of rock friction and fracture to explore the physics of earthquakes.

## 4.2 Focal mechanisms

### 4.2.1 Fault geometry

To describe the geometry of a fault, we assume that the fault is a planar surface across which relative motion occurred during an earthquake. Geological observations of faults that reach the surface show that this is often approximately the case (Fig. 4.2-1), although complexities are common. Similarly, we will see that this assumption is usually (but not always)

**Fig. 4.2-1** Fault cutting across a moraine near Crowley Lake, California. The land in front has dropped relative to the background. (Copyright John S. Shelton.)

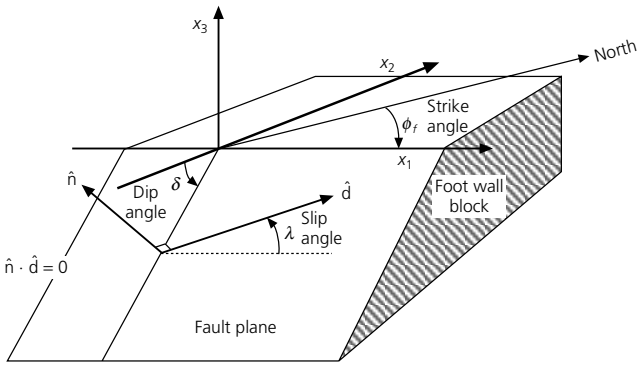


**Fig. 4.2-2** Fault geometry used in earthquake studies. The fault plane, with normal vector $\hat{\mathbf{n}}$, separates the lower, or foot wall, block from the upper hanging wall block (not shown). The slip vector, $\hat{\mathbf{d}}$, describes the motion of the hanging wall block with respect to the foot wall block. The coordinate axes are chosen with $x_3$ vertical and $x_1$ oriented along the fault in the plane of the earth's surface, such that the fault dip angle, $\delta$, measured from the $-x_2$ axis, is less than 90°. The slip angle $\lambda$ is measured between the $x_1$ axis and $\hat{\mathbf{d}}$ in the fault plane. $\phi_f$ is the strike of the fault measured clockwise from north. (After Kanamori and Cipar, 1974. *Phys. Earth Planet. Inter.*, 9, 128–36, with permission from Elsevier Science.)

consistent with seismic data. Thus the fault geometry is described in terms of the orientation of the fault plane and the direction of slip along the plane.

The geometry of this model is shown in Fig. 4.2-2. The fault plane is characterized by $\hat{\mathbf{n}}$, its *normal vector*. The direction of motion is given by $\hat{\mathbf{d}}$, the *slip vector* in the fault plane. The slip vector indicates the direction in which the upper side of the fault, known as the *hanging wall block*, moved with respect to the lower side, the *foot wall block*. Because the slip vector is in the fault plane, it is perpendicular to the normal vector.

Several different coordinate systems are useful in studying faults. One is aligned such that the $x_1$ axis is in the fault *strike* direction, the intersection of the fault plane with the earth's surface. The $x_3$ axis points upward, and the $x_2$ axis is perpendicular to the other two. The dip angle $\delta$ gives the orientation of the fault plane with respect to the surface. Because the $x_1$ axis could be defined in two directions, 180° apart, it is chosen so that the dip measured from the $-x_2$ axis is less than 90°. The direction of motion is represented by the slip angle, $\lambda$, measured counterclockwise in the fault plane from the $x_1$ direction, which gives the motion of the hanging wall block with respect to the foot wall block. To orient this system relative to the geographic one, the fault strike $\phi_f$ is defined as the angle in the plane of the earth's surface measured clockwise from north to the $x_1$ axis.

Alternatively, the orientation of the fault and slip can be described by giving the normal and slip vectors in a geographic coordinate system with $\hat{\mathbf{x}}$ pointing north, $\hat{\mathbf{y}}$ pointing west, and $\hat{\mathbf{z}}$ pointing up. In this coordinate system, the unit normal vector to the fault plane is

$$\hat{\mathbf{n}} = \begin{pmatrix} -\sin\delta\sin\phi_f \\ -\sin\delta\cos\phi_f \\ \cos\delta \end{pmatrix}, \tag{1}$$

and the slip vector, a unit vector in the slip direction, is

$$\hat{\mathbf{d}} = \begin{pmatrix} \cos\lambda\cos\phi_f + \sin\lambda\cos\delta\sin\phi_f \\ -\cos\lambda\sin\phi_f + \sin\lambda\cos\delta\cos\phi_f \\ \sin\lambda\sin\delta \end{pmatrix}. \tag{2}$$

These two different coordinate systems, $(\phi_f, \delta, \lambda)$ and $(\hat{\mathbf{n}}, \hat{\mathbf{d}})$, are useful for different purposes. Some calculations are more easily done with respect to the fault, whereas others are more easily done with respect to geographic directions.

Although the slip direction varies such that the slip angle ranges from 0° to 360°, several basic fault geometries, described by special values of the slip angle, are useful to bear in mind (Fig. 4.2-3). When the two sides of the fault slide horizontally by each other, pure *strike-slip* motion occurs. When $\lambda$ = 0°, the hanging wall moves to the right, and the motion is called *left-lateral*. Similarly, for $\lambda = 180°$, *right-lateral* motion occurs. To tell which is which, look across the fault and see which way the other side moved. The other basic fault geometries describe *dip-slip* motion. When $\lambda = 270°$, the hanging wall slides downward, causing *normal faulting*. In the opposite case, $\lambda = 90°$, and the hanging wall goes upward, yielding *reverse*, or *thrust*, *faulting*.[1] Most earthquakes consist of some combination of these motions and have slip angles between these values. It is thus useful, when thinking about earthquake mechanisms, to remember the three basic faults. As discussed in Section 2.3.5, the basic fault types can be related to the orientations of the principal stress directions.

This discussion brings out the point that although texts typically show vertically dipping strike-slip faults,[2] they are by no means the norm. In fact, as discussed later, the largest earthquakes occur on shallow-dipping thrust faults at subduction zones. Although such faults are harder to study, because the fault trace is generally under water, the same basic principles apply.

Real faults, of course, have finite dimensions and complicated geometries. If we treat a fault as rectangular, the dimension along the strike is called the fault *length*, and the dimension in the dip direction is known as the fault *width*. Actual earthquake fault geometries can be much more complicated than a rectangle. The fault may curve and require a three-dimensional description. Rupture may occur over a long time and consist of several sub-events on different parts of the fault with different orientations. Such complicated seismic events, however, can be treated as a superposition of simple events. Thus, if we

[1] Seismologists often use the terms "reverse" and "thrust" fault interchangeably, whereas structural geologists reserve the term "thrust" for a shallow-dipping reverse fault.

[2] In part because many authors have spent time in California, and in part because they are easy to draw.

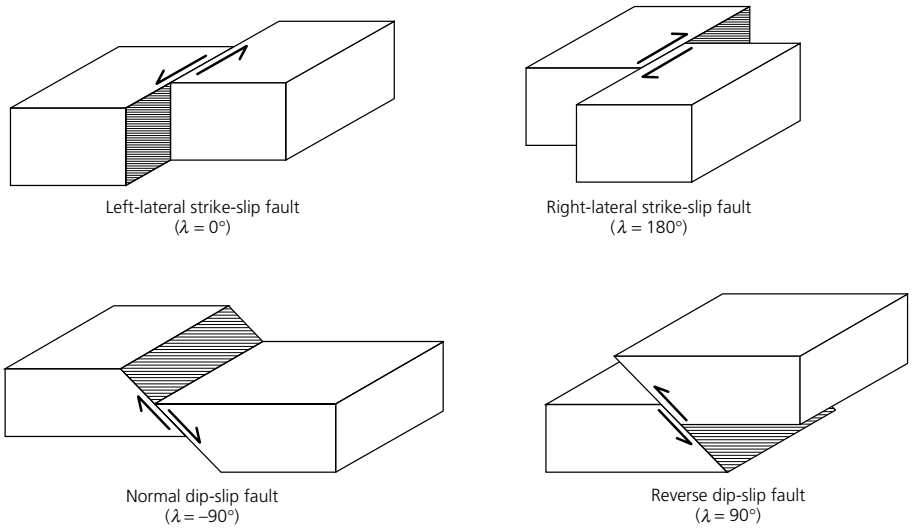


**Fig. 4.2-3** Basic types of faulting. Strike-slip motion can be either right- or left-lateral. Dip-slip faulting can occur as either reverse (thrust) or normal faulting. (Eakins, 1987.)

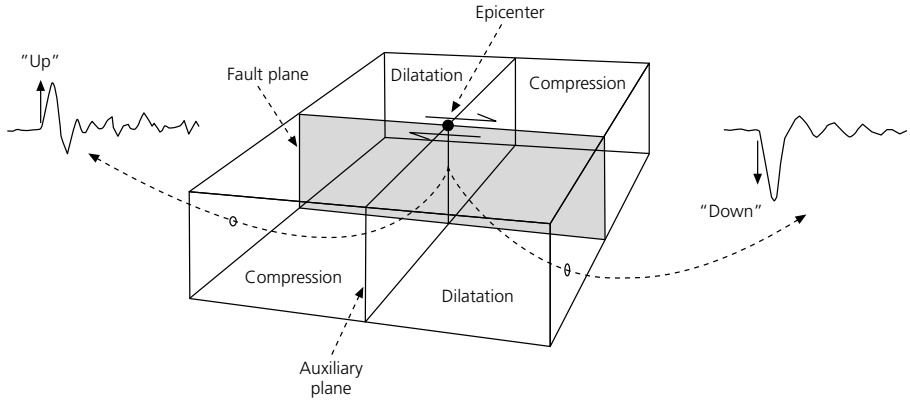


**Fig. 4.2-4** First motions of *P* waves observed at seismometers located in various directions about the earthquake provide information about the fault orientation. The two nodal planes separate regions of compressional and dilatational first arrivals. One nodal plane is the fault plane, and the other is the auxiliary plane, but these data cannot distinguish which is the actual fault plane.

understand the seismic waves generated by a simple, two-dimensional, rectangular fault, we can model those resulting from a more complicated set of ruptures. This application of the principle of superposition is based on the assumption of linear elasticity and is analogous to the way we constructed seismic waves by summing normal modes (Sections 2.2.5 and 2.9).

### 4.2.2 *First motions*

Seismograms recorded at various distances and azimuths are used to study the geometry of faulting during an earthquake, known as the *focal mechanism*. This operation uses the fact that the pattern of radiated seismic waves depends on the fault geometry. The simplest method, which we discuss first, relies on the first motion, or polarity, of body waves. More sophisticated techniques, discussed in the next section, use the waveforms of body and surface waves.

The basic idea is that the polarity (direction) of the first *P*-wave arrival varies between seismic stations at different directions from an earthquake. Figure 4.2-4 illustrates this concept for a strike-slip earthquake on a vertical fault. The first motion is either *compression*, for stations located such that material near the fault moves "toward" the station, or *dilatation*, where the motion is "away from" the station. Thus when a *P* wave arrives at a seismometer from below, a vertical-component seismogram records an upward or downward first motion, corresponding to either compression or dilatation.

The first motions define four quadrants, two compressional and two dilatational. The division between quadrants occurs along the fault plane and a plane perpendicular to it. In these directions, because the first motion changes from dilatation to compression, seismograms show small or zero first motions. These perpendicular planes, called *nodal planes*, separate the compressional and dilatational quadrants. If these planes can be found, the fault geometry is known. A problem is that the first motions from slip on the actual fault plane and from slip on the plane perpendicular to it, the *auxiliary plane*, would be the same, so the first motions alone cannot resolve which plane

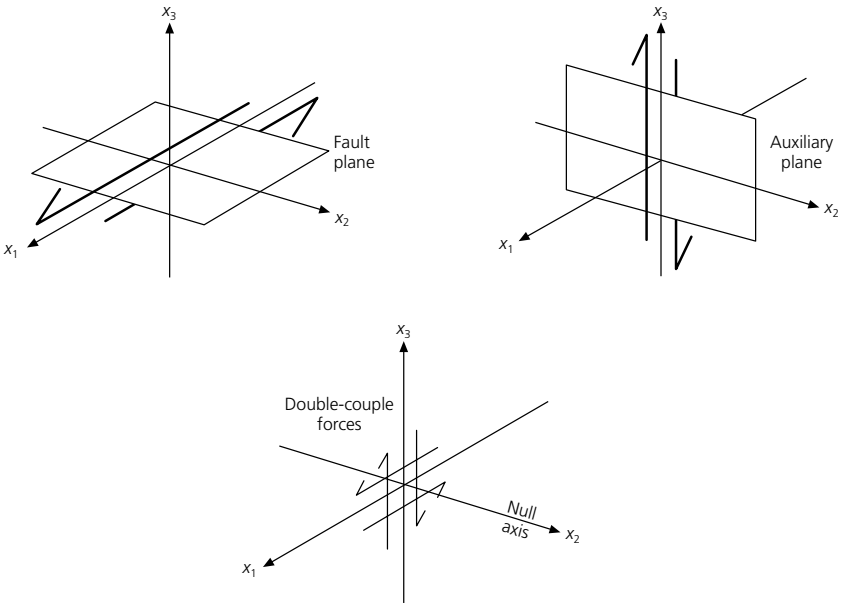


**Fig. 4.2-5** A fault-oriented coordinate system for describing the radiation pattern of an earthquake. The body forces equivalent to the faulting are a pair of force couples acting about the null axis. (After Pearce, 1977.)

is the actual fault plane. However, additional information can often settle the question. Sometimes geologic or geodetic information, such as the trend of a known fault or observations of ground motion, indicates the fault plane. Often, smaller aftershocks following the earthquake occur on, and thus delineate, the fault plane. If the earthquake is large enough, the finite time required for slip to progress along the fault causes variations in the waveforms observed at different directions from the fault, so these *directivity* effects can be used to infer the fault plane.

### *4.2.3 Body wave radiation patterns*

The radiation patterns of *P* and *S* waves, which we will not derive, can be obtained using the theory of seismic sources. The radiation patterns turn out to be those that would be generated by a set of forces with a corresponding geometry. Specifically, the radiation due to motion on the fault plane is what would occur for a pair of force *couples*, pairs of forces with opposite direction a small distance apart. If one couple was oriented in the slip direction with forces on opposite sides of the fault plane, the other couple would be oriented in the corresponding direction on opposite sides of the auxiliary plane. Thus the elastic radiation can be described as resulting from a *double couple*, and these forces are known as the *equivalent body forces* for the fault slip, discussed further in Section 4.4.

It is important to bear in mind that the equivalent forces are only a simple model representing the complex faulting process that actually took place. We can view the faulting as occurring within a "black box" about which the radiated seismic waves provide only limited information. The seismic waves tell us only that some processes within the box produced seismic waves described by the equivalent forces. Often we have other geological and geophysical data, together with (hopefully valid) preconceptions, about the source. In particular, we often (at least believe that we) have good reasons to favor slip on one of the possible fault planes and to interpret the faulting in terms of the regional geology and stress field. Similarly, we interpret aspects of the seismic wave field in terms of simple models of the physics of the faulting process, while recognizing that radiated seismic waves provide only a partial picture.

The radiation patterns of double couples have natural symmetries about the fault plane, and are thus normally written using a coordinate system oriented along the fault. In such a system (Fig. 4.2-5), the fault plane lies in the $x_1$–$x_2$ plane, so its normal is the $x_3$ axis. The slip vector is in the fault plane, parallel to the $x_1$ axis. The slip is such that material above the $x_1$–$x_2$ plane moves in the $+x_1$ direction with respect to the material on the other side. The radiation pattern would be the same if the slip in the $x_3$ direction occurred on the auxiliary plane, which lies in the $x_2$–$x_3$ plane and whose normal is the $x_1$ axis. Thus we can interchange the slip ($x_1$) and normal ($x_3$) directions, so the slip vector on one plane is the normal vector on the other, and vice versa. However, the direction orthogonal to both, known as the *null axis*, is distinct. In this geometry, the equivalent body force double couple acts about the $x_2$ axis, and the forces are oriented along the $x_1$ and $x_3$ directions.

To see how the radiation patterns vary with the direction of the receiver, consider the radiation field in spherical coordinates, where $\theta$ is measured from the $x_3$ axis and $\phi$ is measured in the $x_1$–$x_2$ plane (Figs 4.2-6 and 7). Seismic source theory shows that far from the source, the displacement due to compressional waves, which create the radial ($\hat{\mathbf{e}}_r$) component of the displacement ($u_r$) because their motion is along the propagation direction, is

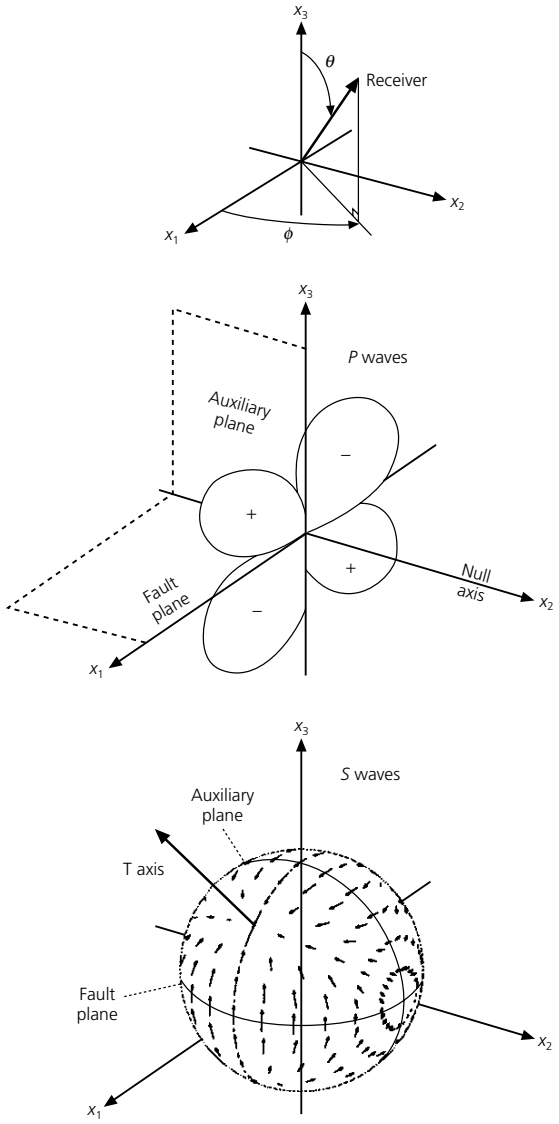


**Fig. 4.2-6** The body wave radiation pattern for a double couple source has symmetry in the spherical coordinate system shown, corresponding to the axes in Fig. 4.2-5. $\theta$ is measured from the $x_3$ axis, the normal to the fault ($x_1$–$x_2$) plane, and $\phi$ is measured in the fault plane. The *P*-wave radiation pattern has four lobes that go to zero at the nodal planes, which are the fault and auxiliary ($x_2$–$x_3$) planes. The *S*-wave radiation pattern describes a vector displacement that does not have nodal planes but is perpendicular to the *P*-wave nodal planes. *S*-wave motion converges toward the T axis, diverges from the P axis, and is zero on the null axis. (After Pearce, 1977, 1980.)

$$u_r = \frac{1}{4\pi\rho\alpha^3 r}\dot{M}(t - r/\alpha)\sin 2\theta\cos\phi. \tag{3}$$

This expression has several parts. The first term is an amplitude term. In an infinite medium, for which this was derived,

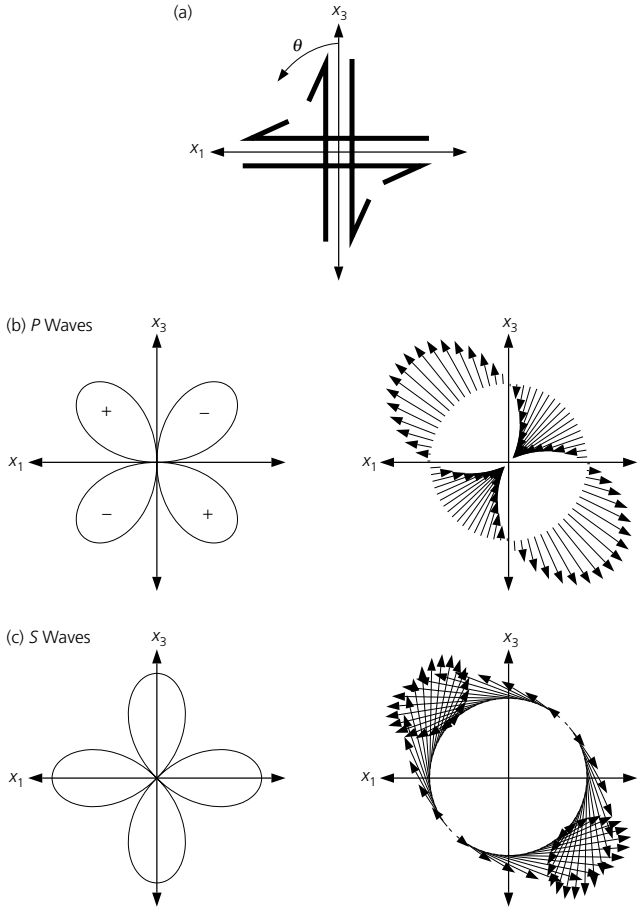


**Fig. 4.2-7** Radiation amplitude patterns of *P* and *S* waves in the $x_1$–$x_3$ plane. a: Fault geometry, showing the symmetry of the double couple about the $x_2$ axis. b: Radiation pattern for *P* waves, showing the amplitude (*left*) and direction (*right*). c: Same as (b), but for *S* waves.

the amplitude would decay as $1/r$. The second term reflects the pulse radiated from the fault, $\dot{M}(t)$, which propagates away at the *P*-wave speed $\alpha$ and arrives at a distance $r$ at time $t - r/\alpha$. $\dot{M}(t)$ is called the seismic moment rate function or *source time function*. It is the time derivative of the *seismic moment function*

$$M(t) = \mu D(t) S(t), \tag{4}$$

which describes the faulting process in terms of the rigidity of the material and history of the slip $D(t)$ and fault area $S(t)$. The latter terms are time-dependent, because they can vary during an earthquake. As discussed in Section 4.6, the best measure of earthquake size and energy release is the static (or scalar) *seismic moment*

$$M_0 = \mu \bar{D} S, \tag{5}$$

where $\overline{D}$ is the average slip (or dislocation) on the fault with area $S$. We often use the seismic moment as a scale factor and write $\dot{M}(t) = M_0 x(t)$, where $x(t)$ is the *source time function*.

The final term, $\sin 2\theta \cos \phi$, describes the $P$-wave radiation pattern. It is four-lobed, with two positive, compressional, lobes and two negative, dilatational, ones. The displacement is zero on the fault ($\theta = 90°$) and auxiliary ($\phi = 90°$) planes. Thus the fault plane and auxiliary plane are nodal planes separating compressional and dilatational quadrants. The maximum amplitudes are between the two nodal planes.

Similarly, the shear wave displacement has two components, $u_\theta \hat{\mathbf{e}}_\theta + u_\phi \hat{\mathbf{e}}_\phi$, where

$$u_\theta = \frac{1}{4\pi\rho\beta^3 r} \dot{M}(t - r/\beta) \cos 2\theta \cos \phi,$$

$$u_\phi = \frac{1}{4\pi\rho\beta^3 r} \dot{M}(t - r/\beta)(-\cos \theta \sin \phi). \qquad (6)$$

Note that the term involving $\dot{M}(t)$ corresponds to waves propagating at the $S$-wave speed $\beta$. As shown in Fig. 4.2-6, the $S$-wave motion does not have nodal planes, but it is perpendicular to the $P$-wave nodal planes and is zero on the null axis. It converges toward the center of the compressional quadrants, which, as we will see shortly, is the location of the **T**, or least compressive stress, axis. It also diverges from the centers of the dilatation quadrants, known as the **P**, or most compressive stress, axis. Thus, although the $S$-wave pattern does not reflect the fault plane as clearly as the $P$-wave pattern, it can also be used to study the fault geometry. An interesting feature of Eqns 3 and 6 is that they show why $S$ waves on seismograms are usually bigger than $P$ waves — the equations predict an average ratio of $\alpha^3/\beta^3$, or about 5.

Because the radiated seismic waves vary as a function of $\theta$ and $\phi$, seismograms recorded at different directions from the earthquake can be used to find the fault geometry. The $P$ wave is the first wave to arrive from an earthquake, so on a seismogram it is an isolated arrival whose polarity is often easy to identify. A set of $P$-wave first motions thus often makes it possible to locate the nodal planes that divide the regions of different polarity. The first $S$ waves are harder to use, because they arrive later in the seismogram and can be buried in a complicated wave train. It is still possible, however, to use the $S$-wave information. One way to do this is to consider the relative amplitudes of the two $S$-wave components.

One additional concept is needed to determine fault plane solutions using the first motions from various seismic stations. The radiation patterns show the displacements that would occur on a sphere with infinitesimal radius about the source. The observations, of course, are at stations some finite distance from the source. We thus need to convert the observations at the stations to hypothetical ones surrounding the source. To do this, recall that seismic waves do not travel in straight lines from the earthquake to a station. Instead, because seismic velocities vary with depth, rays follow curved paths.

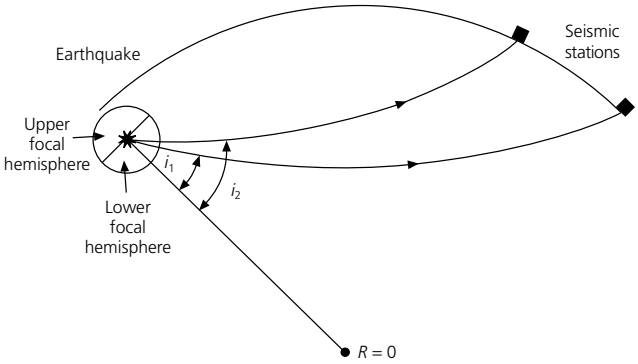


**Fig. 4.2-8** The angle of incidence at the earthquake source is the angle from the vertical at which the ray leaves the source, and thus the angle at which the ray intersects the lower focal hemisphere.

As discussed in Section 3.4, the ray paths are given by Snell's law, which says that the ray parameter is constant along a ray. Thus the ray parameter of the ray arriving at a given distance can be found from the slope of the travel time curve $T(\Delta)$,

$$p = \frac{r \sin i}{v} = \frac{dT}{d\Delta}. \qquad (7)$$

Hence taking $r$ as the radius at the earthquake source and $v$ as the velocity at the source depth, the value of $dT/d\Delta$ for this distance gives the ray's angle of incidence at the source, often called the *take-off angle*. How far a ray travels depends on its take-off angle (Fig. 4.2-8); rays with large take-off angles leave the source closer to the horizontal and travel shorter distances than those with smaller take-off angles.

The distance that a ray has traveled thus gives its take-off angle. Table 4.2-1 is a sample table relating teleseismic travel distances and take-off angles for $P$ waves from a surface-focus earthquake. These distances and angles depend on the velocity model assumed. In teleseismic first motion studies, stations at distances greater than 100° are generally not used because the rays hit the earth's core, and stations for distances closer than 30° are often avoided because the take-off angles depend strongly on the upper mantle velocity structure used. In local earthquake studies, care is taken to ensure that the velocity model is appropriate.

Using such tables, the distances to seismic stations can be converted to take-off angles. Thus the locations of compressions and dilatations can be converted to their positions on the surface of the *lower focal hemisphere*, a hemisphere with infinitesimal radius about the source. A similar approach can be used for data directly above a deep earthquake, where the upper focal hemisphere is a natural representation.

### *4.2.4 Stereographic fault plane representation*

We have seen that fault geometry can be found from the distribution of data on a sphere around the focus. Because plotting

**Table 4.2-1** *P*-wave take-off angles for a surface-focus earthquake.

| Distance (°) | Take-off angle (°) | Distance (°) | Take-off angle (°) | Distance (°) | Take-off angle (°) |
|---|---|---|---|---|---|
| 21 | 36 | 47 | 25 | 73 | 19 |
| 23 | 32 | 49 | 24 | 75 | 18 |
| 25 | 30 | 51 | 24 | 77 | 18 |
| 27 | 29 | 53 | 23 | 79 | 17 |
| 29 | 29 | 55 | 23 | 81 | 17 |
| 31 | 29 | 57 | 23 | 83 | 16 |
| 33 | 28 | 59 | 22 | 85 | 16 |
| 35 | 28 | 61 | 22 | 87 | 15 |
| 37 | 27 | 63 | 21 | 89 | 15 |
| 39 | 27 | 65 | 21 | 91 | 15 |
| 41 | 26 | 67 | 20 | 93 | 14 |
| 43 | 26 | 69 | 20 | 95 | 14 |
| 45 | 25 | 71 | 19 | 97 | 14 |

*Source*: After Pho and Behe (1972).

on a piece of paper is easier than plotting on a sphere, a *stereographic projection* that transforms a hemisphere to a plane is used to plot the data. The graphic construction that does this is a *stereonet* (Fig. 4.2-9).[3] On this net, the azimuth is shown by the numbers from 0° to 360° around the circumference. The dip angles are shown by the numbers from 90° to 0° along the net's equator. The angle 90°, straight down, hits the middle of the net, whereas 0°, the horizontal direction, is at the edge.

To see how to use this net, consider how planes through the center of the focal sphere appear (Fig. 4.2-10). A vertically dipping, N–S-striking, plane intersects the hemisphere such that it plots as a straight line through the center of the net. A N–S-striking plane with a different dip intersects the net edge at 0° and 180°, but intersects the equator at a position corresponding to the dip. For example, planes dipping 70°E and 60° W intersect the equator at the 70°E and 60°W marks. Thus, *meridians* on the net (the curves going from the top to the bottom) represent N–S-striking planes with different dips.

Planes striking in other azimuths are plotted in a similar way (Fig. 4.2-11) by rotating the stereonet.[4] Thus, a plane striking at an angle $\phi$ (measured clockwise from north) is plotted by rotating the stereonet so that the vertical (N–S) axis points in the $\phi$ direction. The plane with the desired dip is now a meridian, so it can be found using the scale along the equator. After plotting the plane by tracing the appropriate meridian, we rotate the net back to its original orientation. Hence planes striking in azimuths other than N–S appear as meridians relative to their strike direction, with the appropriate dip. All of these meridians are thus great circles, the curves formed when a plane through the center of the sphere intersects the surface of the sphere.

[3] Seismologists generally use an equal-area or Schmidt projection, rather than an equal-angle or Wulff projection. The techniques used are the same for the two.

[4] This can be done either by the traditional method, rotating a piece of tracing paper over a stereonet, or by using a computer program that plots points and planes on a stereonet.

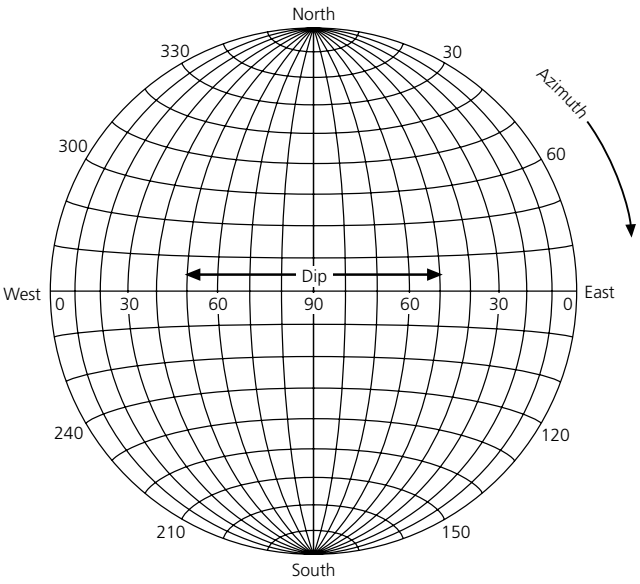


**Fig. 4.2-9** A stereonet used to display a hemisphere on a flat surface. The azimuth is shown by the numbers around the circumference, and dip angles are shown by the numbers along the equator.

We can also plot planes perpendicular to a given plane. To do this, rotate the stereonet so that the plane lies on a meridian, and find the point on the equator 90° from the intersection of the plane with the equator (Fig. 4.2-12). This point is the *pole* for the plane, because it represents the point at which the normal to the plane intersects the sphere. Any plane perpendicular to the first plane contains the normal, and hence must pass through the pole. To draw such perpendicular planes, remember that an arbitrary curve on the stereonet does not represent a

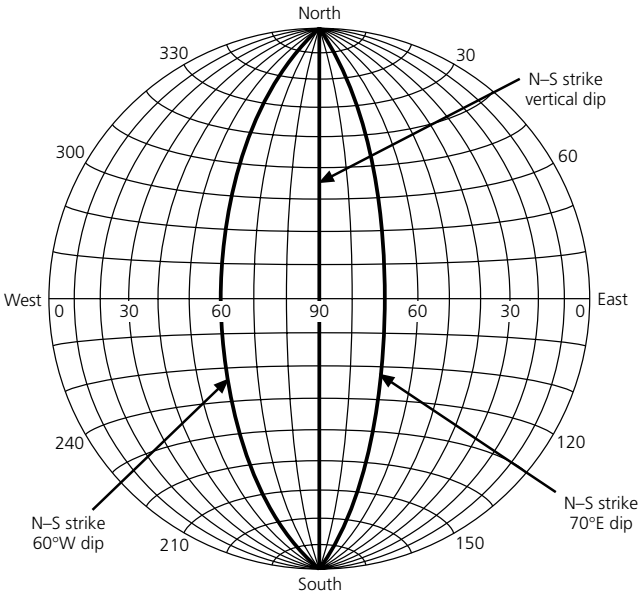


**Fig. 4.2-10** Three planes striking N–S on a stereonet. The meridians (curves going from the top to the bottom) represent N–S-striking planes with different dips.

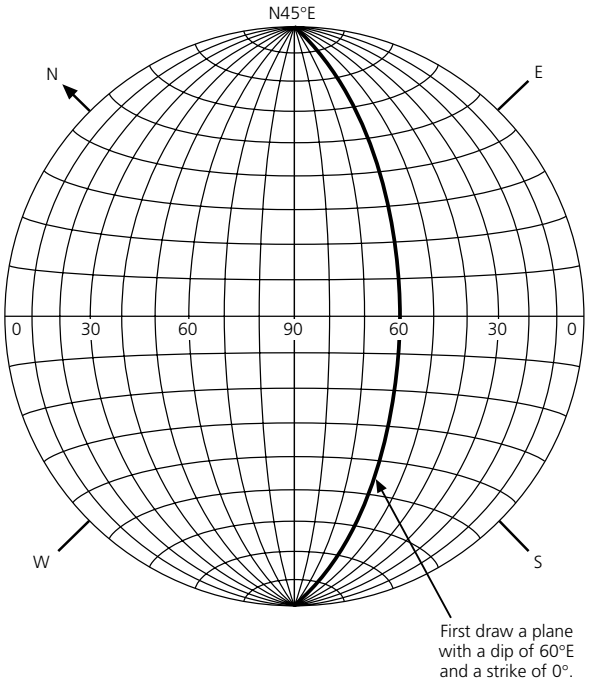


plane; only meridians are projections of planes. We thus rotate the net in the desired direction and trace meridians going through the pole.

To determine focal mechanisms, we plot the points where rays intersect the focal sphere, so that the nodal planes can be found. For example, to plot the point corresponding to a ray whose azimuth is 40° and whose take-off angle is 60°, we first rotate the net, placing the equator along azimuth 40°. Because take-off angles $i$ are measured from the vertical, they correspond to dips of $90 - i$. We thus mark the point with dip 30°E, and rotate the net back so that north is at the top (Fig. 4.2-13).

We can use these ideas to determine the focal mechanism from a set of *P*-wave first motions. First, we find the polarities of the first arrivals at seismic stations. Each station corresponds to a point on the focal sphere with the same azimuth and an incidence angle corresponding to the ray that emerged there. We then plot the location of each station on the stereonet and mark whether the first motion is dilatation or compression. Next, by rotating the tracing paper or using a stereonet program, we find the nodal planes that best separate the compressions from the dilatations. In doing this, we ensure that the two planes are orthogonal, with each one passing through the pole to the other. Provided the distribution of stations on the focal sphere is adequate, we can find the nodal planes, which are the fault plane and the auxiliary plane.

Different types of faults appear differently on a stereonet (Fig. 4.2-14). The black and white quadrants, representing

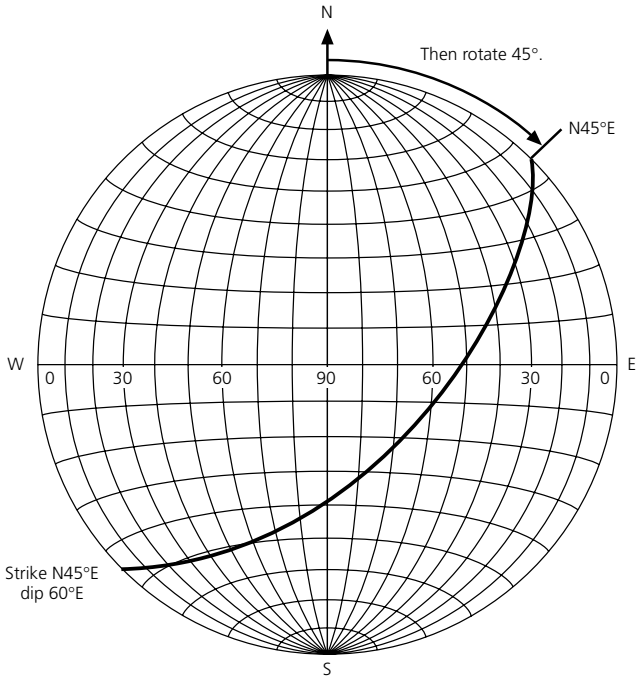


**Fig. 4.2-11** To plot a plane striking N45°E and dipping 60°E, rotate the stereonet (or tracing paper above it) so that the strike is at the top and the dip can be measured along the equator. After plotting the appropriate meridian, rotate the net back to the geographic orientation with north at the top.

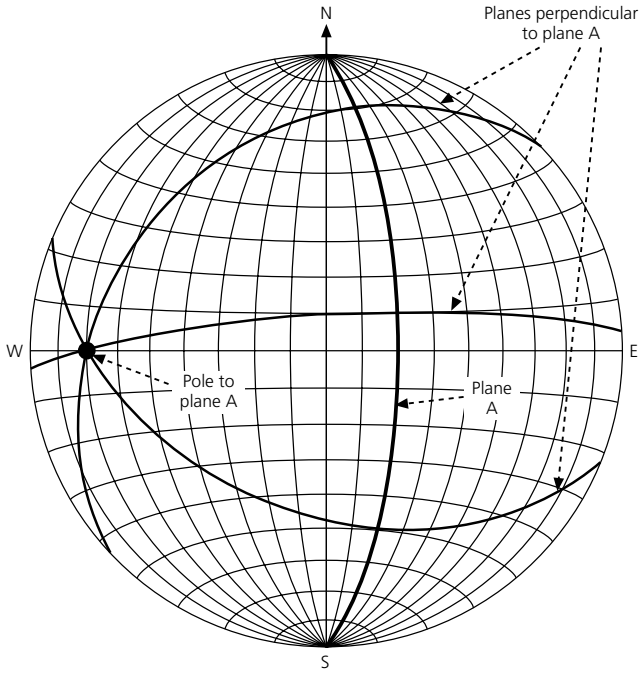


**Fig. 4.2-12** Plotting perpendicular planes on a stereonet. First, rotate the first plane's strike to the top of the stereonet, and plot the plane. Next, find the pole, the point on the equator 90° away. Any plane through the pole is perpendicular to the first plane. Several such planes, with different strikes and dips, are shown.

compression and dilatation, show the fault geometry. A four-quadrant "checkerboard" indicates pure strike-slip motion on a vertical fault plane. The motion would be right-lateral if one plane is the fault plane, and left-lateral on the other. As we mentioned earlier, often the distribution of aftershocks or geologic information (or prejudices) is used to infer which was the actual fault plane, and thus the sense of slip. A pure dip-slip fault that dips at 45° (the fourth quadrant is on the upper focal hemisphere) gives a three-quadrant "beachball." The center region is compressional for a thrust fault, and dilatational for a normal fault. The difference reflects the different direction of fault motion, as the side-view cartoon shows. For a dip-slip rupture on a vertical fault, only two quadrants of the "beachball" are visible, because the others are on the upper focal hemisphere.

The pattern is a little more complicated for oblique-slip faults with a mixture of strike-slip and dip-slip motion. The mechanisms in Fig. 4.2-15 have the same N–S-striking, 45°E-dipping fault plane, but with slip directions varying from pure thrust, to pure strike-slip, to pure normal. Thus the auxiliary plane varies but always passes through the normal to the fault plane, and the slip vector can be found because it is the normal to the auxiliary plane, and thus is in the fault plane (Fig. 4.2-5).

It is important to bear in mind that although the focal mechanisms look different, they reflect the same four-lobed *P*-wave radiation pattern (Fig. 4.2-6). However, because the fault

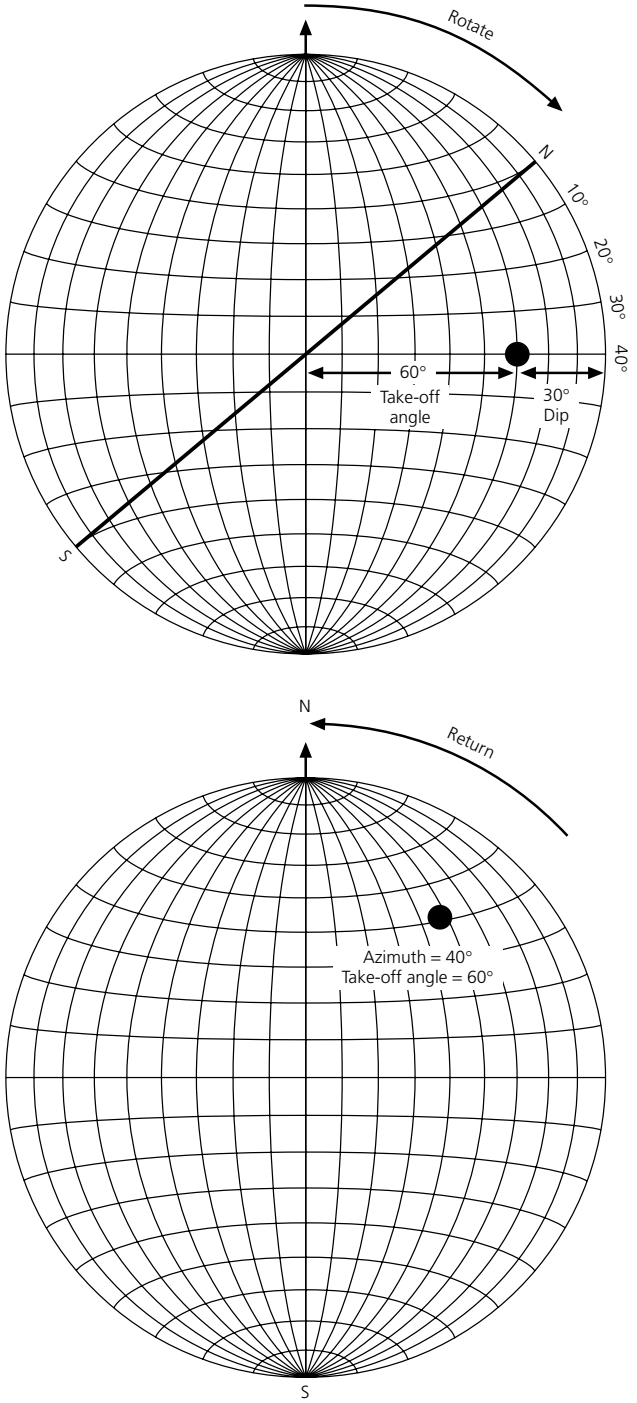


**Fig. 4.2-13** To plot a point on a stereonet, rotate the azimuth of the point to the equator, measure the take-off angle from the vertical (or equivalently the dip from horizontal), plot the point and rotate back to the geographic orientation with north at the top.

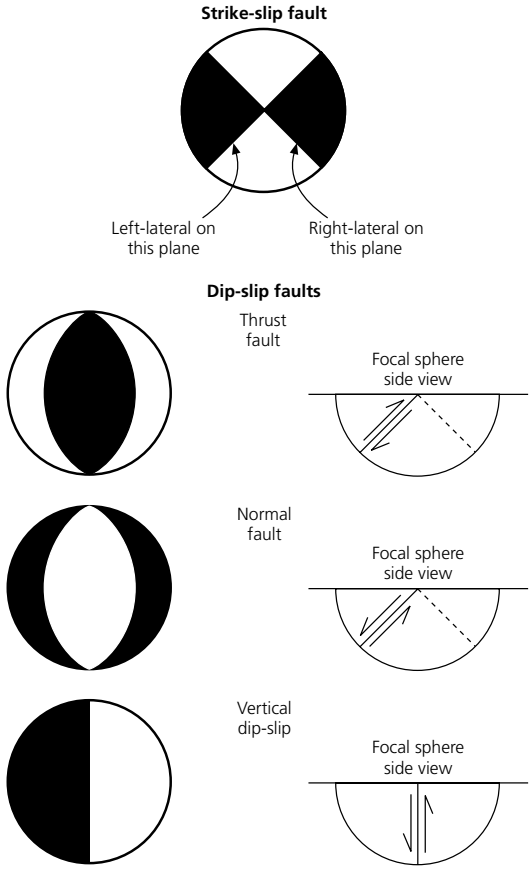


**Fig. 4.2-14** Focal mechanisms for earthquakes with various fault geometries. Compressional quadrants are black. The strike-slip mechanism is for pure strike-slip motion on a vertical fault plane, which could be oriented either NE–SW or NW–SE. The pure dip-slip mechanisms are for faults striking N–S.

plane and slip direction are oriented differently relative to the earth's surface, the projections of the radiation pattern lobes on the lower focal hemisphere differ.[5] Pure dip-slip motion on a 45° dipping fault has two lobes along the vertical axis, so the nodal planes dip at 45°. By contrast, pure strike-slip motion on a vertical plane has lobes in the plane of the surface, and the null axis is vertical.

A common use of earthquake focal mechanisms is to infer stress orientations in the earth. As discussed in Section 2.3.4, a simple model predicts that the faulting occurs on planes 45° from the maximum and minimum compressive stresses. Equivalently, these stress directions are halfway between the nodal planes. Thus the maximum compressive (P) and minimum compressive stress (T) axes can be found by bisecting the dilatational and compressional quadrants, respectively

[5] This concept can be seen by marking the *P*-wave quadrants on a ball and rotating it. For additional insight, the *S*-wave radiation pattern (Fig. 6) can also be marked on the ball.

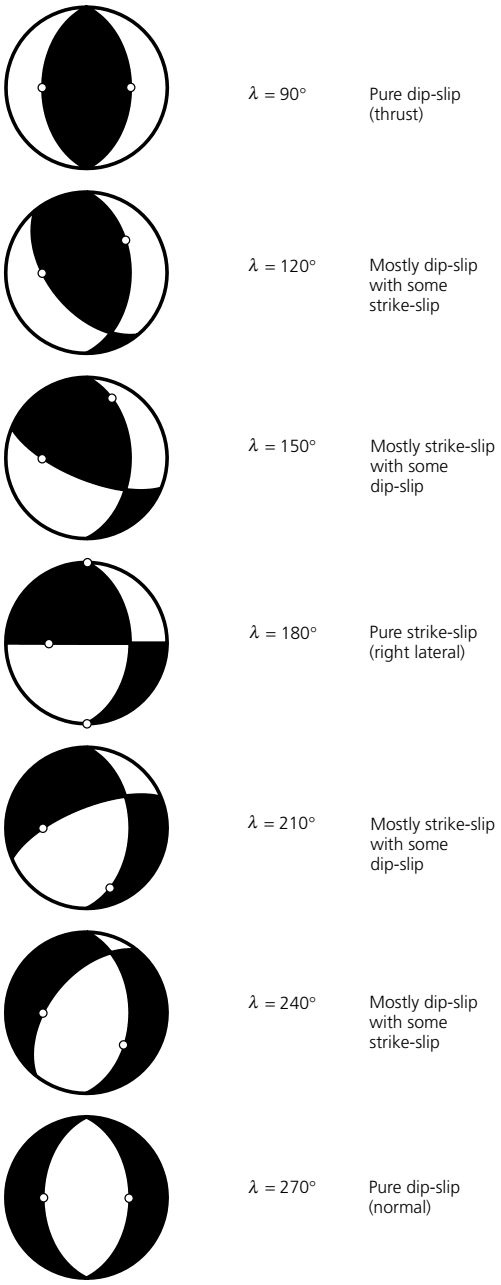


**Fig. 4.2-15** Focal mechanisms for earthquakes with the same N–S-striking fault plane, but with slip angles varying from pure thrust, to pure strike-slip, to pure normal faulting.

(Fig. 4.2-16). Although T is called the "tension" axis, it is actually the minimum compressive stress, because compression occurs at depth in the earth. The intermediate stress axis, known as the B or null axis, is perpendicular to both the T and the P axes. This direction is also perpendicular to both the slip

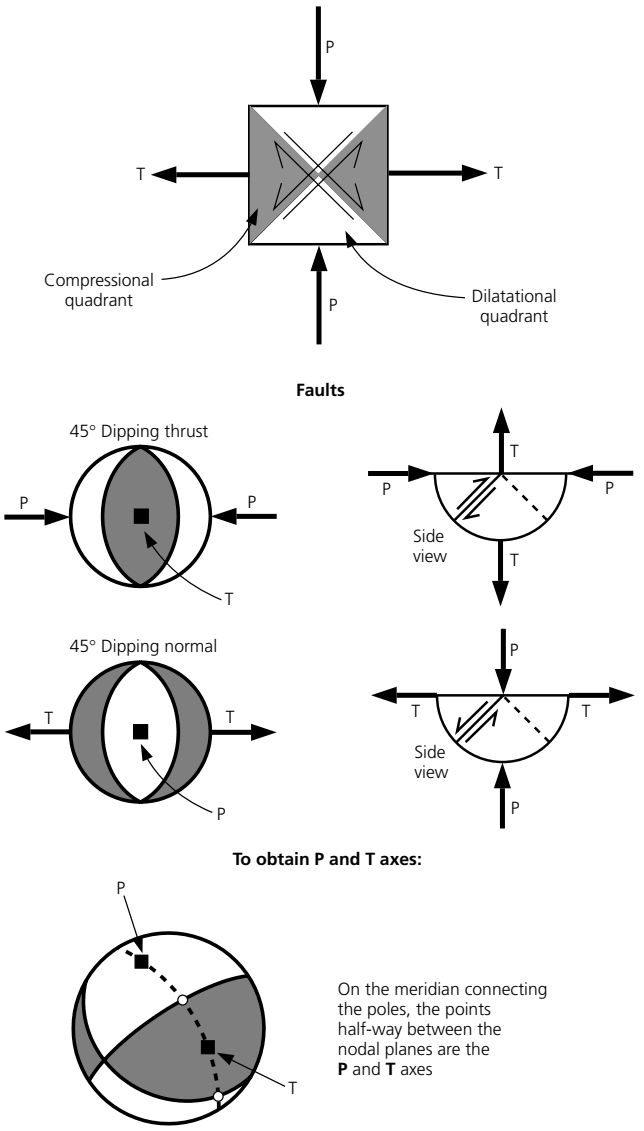


**Fig. 4.2-16** Cartoon illustrating the relation between fault planes and the maximum compressive principal stress (P) and the minimum compressive stress (T) axes. The P and T axes can be found by bisecting the dilatational and compressional quadrants, respectively. On a stereonet, this is done by using the great circle (meridian) connecting the poles for the two nodal planes and finding the point halfway between them.

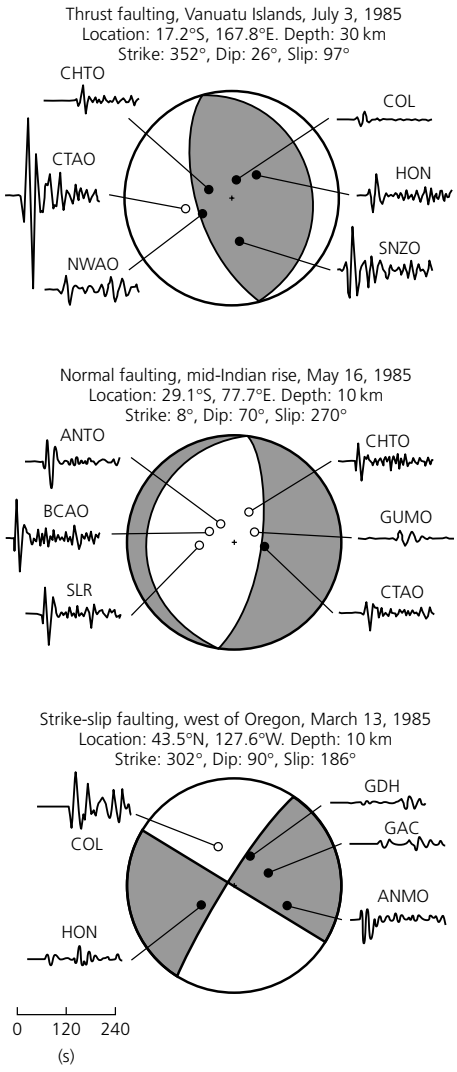


**Fig. 4.2-17** Focal mechanisms and some seismograms for three different earthquakes. Compressional quadrants are shown shaded.

and the normal vectors, and is the intersection of the two nodal planes.

To bisect the angle between the two nodal planes on the stereonet, we find the poles for the two planes (each of which is in the other plane), draw the great circle (meridian) connecting them, and mark the point on it halfway between the poles (Fig. 4.2-16). We can thus infer stress directions from a focal mechanism. Different fault types correspond to different orientations of the stress axes, as noted in Fig. 2.3-9. If the P axis is vertical, the fault plane dips at 45°, and normal faulting occurs. If, instead, the T axis is vertical, the fault geometry is the same, but reverse faulting occurs. When the null axis is vertical, strike-slip motion occurs on a fault plane 45° from the maximum principal stresses, which are in the plane of the surface.

Figure 4.2-17 shows the focal mechanisms and a few of the seismograms for three earthquakes. Note that in some cases the first arrival is small and difficult to identify. This is especially likely when the station is near a nodal plane, where the amplitude is small. It is also worth noting that often many stations plot near the center of the focal sphere, because they are at large distances from the source, so rays to them have small angles of incidence. As a result, it is sometimes hard to constrain nodal

planes, especially if the plane is far from the vertical, as in the dip-slip examples shown. In such cases, information about the waveforms as well as the polarity of the waves is used, as discussed later.

### *4.2.5 Analytical representation of fault geometry*

In many applications, including seismic moment tensor analysis, which we discuss shortly, it is useful to have analytic expressions for the relations between the fault plane, the auxiliary plane, and the stress axes. In Section 4.2.1, we expressed the fault normal and slip vectors in a geographic coordinate system, such that for a fault with strike $\phi_f$, dip angle $\delta$, and slip angle $\lambda$ the fault normal and slip vectors are

$$\hat{\mathbf{n}} = \begin{pmatrix} -\sin\delta\sin\phi_f \\ -\sin\delta\cos\phi_f \\ \cos\delta \end{pmatrix},$$

$$\hat{\mathbf{d}} = \begin{pmatrix} \cos\lambda\cos\phi_f + \sin\lambda\cos\delta\sin\phi_f \\ -\cos\lambda\sin\phi_f + \sin\lambda\cos\delta\cos\phi_f \\ \sin\lambda\sin\delta \end{pmatrix}. \tag{8}$$

Because the null (or B) axis is orthogonal to the fault normal and slip vectors, a unit vector in this direction can be written

$$\hat{\mathbf{b}} = \hat{\mathbf{n}} \times \hat{\mathbf{d}} = \begin{pmatrix} -\sin\lambda\cos\phi_f + \cos\lambda\cos\delta\sin\phi_f \\ \sin\lambda\sin\phi_f + \cos\lambda\cos\delta\cos\phi_f \\ \cos\lambda\sin\delta \end{pmatrix}. \tag{9}$$

Similarly, to find vectors $\mathbf{p}$ and $\mathbf{t}$ along the P and T axes, note that they are in the plane containing $\hat{\mathbf{d}}$ and $\hat{\mathbf{n}}$ and lie halfway between them, so

$$\begin{aligned} &\mathbf{t} = \hat{\mathbf{n}} + \hat{\mathbf{d}} \quad t_i = n_i + d_i, \\ &\mathbf{p} = \hat{\mathbf{n}} - \hat{\mathbf{d}} \quad p_i = n_i - d_i, \\ &\hat{\mathbf{b}} = \hat{\mathbf{n}} \times \hat{\mathbf{d}} \quad b_i = \varepsilon_{ijk} n_j d_k. \end{aligned} \tag{10}$$

It turns out that the null axis is perpendicular to both the P and the T axes. To see this, we use the cross-product (Eqn A.3.43) to form a vector perpendicular to both axes,

$$\begin{aligned} (1/2)(\mathbf{t}\times\mathbf{p}) &= (1/2)(\hat{\mathbf{n}} + \hat{\mathbf{d}}) \times (\hat{\mathbf{n}} - \hat{\mathbf{d}}) = (\varepsilon_{ijk}/2)(n_j + d_j)(n_k - d_k) \\ &= (\varepsilon_{ijk}/2)(n_j n_k - n_j d_k + d_j n_k - d_j d_k), \end{aligned} \tag{11}$$

and simplify, using

$$\begin{aligned} &\hat{\mathbf{n}} \times \hat{\mathbf{n}} = \varepsilon_{ijk} n_j n_k = 0, \quad \hat{\mathbf{d}} \times \hat{\mathbf{d}} = \varepsilon_{ijk} d_j d_k = 0, \\ &\varepsilon_{ijk} d_j n_k = -\varepsilon_{ijk} n_j d_k, \end{aligned} \tag{12}$$

to see that

$$(1/2)(\mathbf{t}\times\mathbf{p}) = -\varepsilon_{ijk} n_j d_k = -(\hat{\mathbf{n}} \times \hat{\mathbf{d}}), \tag{13}$$

which is just the negative of a unit vector along the null axis, $\mathbf{b}$. Thus either the fault normal vector, slip vector, and null axis or the P, T, and B (null) axes can be used for an orthogonal coordinate system.

The relationship between the fault and auxiliary planes can be derived from the fact that the slip vector, which lies in the fault plane, is the normal to the auxiliary plane and vice versa. Thus if $\hat{\mathbf{n}}_1$, $\hat{\mathbf{d}}_1$ and $\hat{\mathbf{n}}_2$, $\hat{\mathbf{d}}_2$ are the fault normal and slip vectors for the two nodal planes,

$$\hat{\mathbf{d}}_1 = \hat{\mathbf{n}}_2 \quad \text{and} \quad \hat{\mathbf{d}}_2 = \hat{\mathbf{n}}_1. \tag{14}$$

Writing out $\hat{\mathbf{d}}_1 = \hat{\mathbf{n}}_2$ by components,

$$\begin{pmatrix} \cos\lambda_1\cos\phi_{f_1} + \sin\lambda_1\cos\delta_1\sin\phi_{f_1} \\ -\cos\lambda_1\sin\phi_{f_1} + \sin\lambda_1\cos\delta_1\cos\phi_{f_1} \\ \sin\lambda_1\sin\delta_1 \end{pmatrix} = \begin{pmatrix} -\sin\delta_2\sin\phi_{f_2} \\ -\sin\delta_2\cos\phi_{f_2} \\ \cos\delta_2 \end{pmatrix}. \tag{15}$$

The corresponding relation between $\hat{\mathbf{n}}_1$ and $\hat{\mathbf{d}}_2$ is found simply by interchanging subscripts.

These equations relate the strike, dip, and slip angles for one plane to the other. To use them, we multiply the first by $\cos\phi_{f_1}$ and the second by $\sin\phi_{f_1}$, and subtract them to find

$$\cos\lambda_1 = \sin\delta_2\sin(\phi_{f_1} - \phi_{f_2}), \tag{16}$$

or, equivalently,

$$\cos\lambda_2 = \sin\delta_1\sin(\phi_{f_2} - \phi_{f_1}). \tag{17}$$

We also have the third equation

$$\cos\delta_2 = \sin\lambda_1\sin\delta_1, \tag{18}$$

or, equivalently,

$$\cos\delta_1 = \sin\lambda_2\sin\delta_2. \tag{19}$$

An additional constraint comes from the fact that the two nodal planes are perpendicular:

$$\hat{\mathbf{n}}_1 \cdot \hat{\mathbf{n}}_2 = 0, \tag{20}$$

so

$$\begin{aligned} &\sin\delta_1\sin\phi_{f_1}\sin\delta_2\sin\phi_{f_2} + \sin\delta_1\cos\phi_{f_1}\sin\delta_2\cos\phi_{f_2} \\ &\quad + \cos\delta_1\cos\delta_2 = 0, \\ &\sin\delta_1\sin\delta_2\cos(\phi_{f_1} - \phi_{f_2}) + \cos\delta_1\cos\delta_2 = 0; \end{aligned} \tag{21}$$

or

$$\tan\delta_1\tan\delta_2\cos(\phi_{f_1} - \phi_{f_2}) = -1. \tag{22}$$

These equations allow us to find the the second nodal plane and the slip vector on it ($\phi_{f_2}$, $\delta_2$, $\lambda_2$) from the first nodal plane and the slip on it ($\phi_{f1}$, $\delta_1$, $\lambda_1$). The hard part, getting the angles in the appropriate quadrants, can be done by first finding $\delta_2$ from Eqn 18, and then finding sin $\lambda_2$ from Eqn 19 and cos $\lambda_2$ by combining Eqns 16 and 17. Given both sine and cosine, $\lambda_2$ can be placed in the correct quadrant. We then find $\phi_{f_2}$ from Eqns 22 and 16. Finally, if $90° < \delta_2 < 180°$, we change ($\phi_{f_2}$, $\delta_2$, $\lambda_2$) to ($180° + \phi_{f_2}$, $180° - \delta_2$, $360° - \lambda_2$).

If the nodal planes have been found from first motions using a stereonet, the situation differs because the strike and dip of both planes are known, but the slip angles are not. We then choose one nodal plane and find the slip angle on it. This can be done using Eqns 16 and 18 to find cos $\lambda_1$ and sin $\lambda_1$, and then placing $\lambda_1$ in the correct quadrant.

## 4.3 Waveform modeling

As noted in the previous section, *P*-wave first motions are often inadequate to constrain focal mechanisms. Additional information is obtained by comparing the observed body and surface waves to theoretical, or *synthetic*, waveforms computed for various source parameters, and finding a model that best fits the data, either by forward modeling or by inversion. Waveform analysis also gives information about the earthquake depths and rupture processes which cannot be extracted from the first motions. We discuss such analysis first for body waves and then for surface waves.

### *4.3.1 Basic model*

To generate synthetic waveforms, we regard the ground motion recorded on a seismogram as a combination of factors: the earthquake source, the earth structure through which the waves propagated, and the seismometer. Each factor can be thought of as an operation whose effects depend on the frequency of the seismic waves. Hence it is often useful to think of the seismogram $u(t)$ in terms of its Fourier transform $U(\omega)$, which represents the contribution of the different frequencies:

$$u(t) = \frac{1}{2\pi}\int_{-\infty}^{\infty} U(\omega)e^{i\omega t}d\omega \qquad U(\omega) = \int_{-\infty}^{\infty} u(t)e^{-i\omega t}dt \tag{1}$$

As as in earlier discussions (Sections 2.8, 3.3, 3.7), we use the Fourier transform and related concepts while deferring more general treatment of Fourier analysis to Chapter 6. The essence of this approach is that we represent a seismogram or individual factors that make it up either as a time series or by its Fourier transform, depending on which is more convenient, and switch back and forth using the transform and inverse transform relations.

This approach to generating synthetic seismograms from earthquakes is conceptually the same as that discussed in Section 3.3.6 for reflection seismograms. There, we described the combined effect of various factors as the *convolution* of time series representing each factor. Recall that the convolution of two time series $w(t)$ and $r(t)$ is written

$$s(t) = w(t) * r(t) = \int_{-\infty}^{\infty} w(t-\tau)r(\tau)d\tau. \tag{2}$$

Thus a seismogram $u(t)$ can be written

$$u(t) = x(t) * e(t) * q(t) * i(t), \tag{3}$$

where $x(t)$ is the source time function, the "signal" the earthquake puts into the ground, $e(t)$ and $q(t)$ represent the effects of earth structure, and $i(t)$ describes the instrument response of the seismometer. We also noted (and will prove in Section 6.3.1) that convolution in the time domain is equivalent to multiplication in the frequency domain, so Eqn 3 can be written as the product of Fourier transforms of the four factors

$$U(\omega) = X(\omega)E(\omega)Q(\omega)I(\omega). \tag{4}$$

Each factor can be described in the time domain or the frequency domain. For example, the seismogram depends on how the seismometer responds to ground motion of different frequencies. Figure 4.3-1 (*top*) shows the instrument response, the amplification of a signal as a function of period, for a long-period seismometer. Ground motion with periods around the peak response ($T = 15$ s) is enhanced relative to that at longer or shorter periods. As discussed in Section 6.6, seismometer responses differ; some have peak response at short (e.g., 1 s) periods, whereas others have better response at longer periods. The seismometer response can also be described in the time domain by taking its inverse Fourier transform (Fig. 4.3-1, *bottom*). The resulting time series, $i(t)$, is the *impulse response*, describing how the seismometer responds to a sharp impulse. For the seismometer illustrated in Fig. 4.3-1, the impulse response has a sharp initial peak, followed by a smaller "backswing."

In this formulation, the effects of earth structure are divided into two factors. One, $e(t)$, gives the effect of reflections and conversions of seismic waves at different interfaces along the ray path and the effect of geometric spreading of the rays due to the velocity structure (Section 3.4.2). All these effects are elastic wave phenomena. There is also anelastic *attenuation* described by $q(t)$, whereby some of the seismic waves' mechanical energy is lost by conversion into heat. Attenuation, discussed in Section 3.7, is illustrated by the decay with time of a damped harmonic oscillation with frequency $\omega$:

$$f(t) = A e^{i\omega t} e^{-\omega t/2Q}. \tag{5}$$

The quality factor $Q$ characterizes the attenuation: the amplitude decays by $e^{-1}$ in a time $2Q/\omega$ (Fig. 3.7-11), so the higher